Resonant Electron Scattering by Defects in Single-Walled Carbon Nanotubes

Marc Bockrath, *et al.*

Science **291**, 283 (2001);
DOI: 10.1126/science.291.5502.283

Science (print ISSN 0036-8075; online ISSN 1095-9203) is published weekly, except the last week in December, by the American Association for the Advancement of Science, 1200 New York Avenue NW, Washington, DC 20005.

Resonant Electron Scattering by Defects in Single-Walled Carbon Nanotubes

Marc Bockrath,[1] Wenjie Liang,[2] Dolores Bozovic,[1] Jason H. Hafner,[2] Charles M. Lieber,[2] M. Tinkham,[1] Hongkun Park[2]*

We report the characterization of defects in individual metallic single-walled carbon nanotubes by transport measurements and scanned gate microscopy. A sizable fraction of metallic nanotubes grown by chemical vapor deposition exhibits strongly gate voltage–dependent resistance at room temperature. Scanned gate measurements reveal that this behavior originates from resonant electron scattering by defects in the nanotube as the Fermi level is varied by the gate voltage. The reflection coefficient at the peak of a scattering resonance was determined to be about 0.5 at room temperature. An intratube quantum dot device formed by two defects is demonstrated by low-temperature transport measurements.

Single-walled carbon nanotubes (SWNTs) have emerged as an attractive material for molecular electronic applications (*1, 2*). Depending on their diameter and chirality, SWNTs can be either one-dimensional metals or semiconductors, and a variety of electronic devices based on SWNTs, such as single-electron transistors (*3, 4*) and field-effect transistors (*5, 6*), have been realized experimentally. Electronic devices based on SWNTs can serve as a basis for other related applications as well, such as chemical sensors (*7*) and electromechanical devices (*8, 9*).

Most experimental and theoretical investigations to date have focused on defect-free SWNTs with perfect honeycomb carbon arrangements (*1, 2*). Recent theoretical calculations have shown, however, that structural defects in the underlying carbon lattice, such as topological defects, vacancies, and chemical modifications, can substantially modify the electronic properties of SWNTs (*10–17*). Experimental characterizations of nanotube defects are only beginning to emerge (*18–20*), and many theoretical predictions remain to be tested.

Here, we report transport and scanned gate investigations of defects in individual metallic SWNTs grown by chemical vapor deposition (CVD) (*21, 22*). These measurements provide evidence for resonant electron scattering by individual defects in SWNTs, confirming previous theoretical predictions for structural defects in SWNTs (*11, 15–17*). The transport measurements also show that the defects can impart unique electronic functionality to SWNTs, as demonstrated by the formation of an intratube quantum dot with gate-tunable barriers (*14*).

Isolated SWNTs were synthesized by CVD with the procedure reported previously at temperatures ranging from 700° to 900°C (*21–23*). Both transmission electron and atomic force microscopic (AFM) characterizations reveal that SWNTs with diameters between 1 and 3 nm are predominantly produced in this experimental condition, although some multiwalled nanotubes with a diameter of ≥2 nm are also produced. Nanotubes with a diameter of ≤1 nm were located in relation to alignment marks, and electrical leads were defined by electron-beam lithography (Fig. 1C). The selection of small-diameter nanotubes ensures that the samples studied are predominantly individual SWNTs.

Electrical characterization was performed as a function of bias voltage (V_{sd}) and gate voltage (V_g). The degenerately doped silicon substrate acted as a gate electrode to modulate the charge density within the nanotubes. Nanotube devices were classified as semiconducting or metallic on the basis of their resistance-V_g behavior at room temperature (*5, 24*). Semiconducting nanotube devices became insulating at large positive V_g values (*5*), whereas metallic nanotube devices showed finite resistance over the experimentally accessible V_g range ($|V_g| \leq 70$ V) (*24*). Some metallic nanotubes exhibited resistance independent of V_g, as expected for one-dimensional metal (*24*). Surprisingly, however, ~60% of >50 metallic nanotube devices showed resistance that changed substantially with V_g (Fig. 1A). Despite the resistance change observed in these devices, they could not be made insulating by varying V_g, indicating that they do not contain semiconducting segments.

Scanned gate microscopy (SGM) was used to study the origin of the V_g-dependent resistance (*25, 26*). A conductive AFM tip with an applied voltage (V_{tip}) was scanned over the sample at a fixed height, and an image was obtained by plotting the device resistance as a function of tip position (Fig. 1B). The tip voltage induces a local charge accumulation near the tip, which shifts the local Fermi level (ε_{loc}) in the nanotube (*25*). The SGM images therefore map the resistance change of a device as ε_{loc} is tuned by V_{tip} and the tip position.

SGM images obtained from a representative device (D1) at room temperature are shown in Fig. 1, D through F. At $V_{tip} = 3$ V, two dark spots appear along the nanotube (Fig. 1D); these dark spots represent increased device resistance, signifying the presence of localized electron scattering centers in the nanotube (*26*). When V_{tip} is increased further, the dark spots expand into dark ring-like features [scanned gate (SG) rings] with a diameter proportional to V_{tip} (Fig. 1, E and F). New dark spots and smaller SG rings also appear along the nanotube with a typical separation of ~150 nm. The observation of

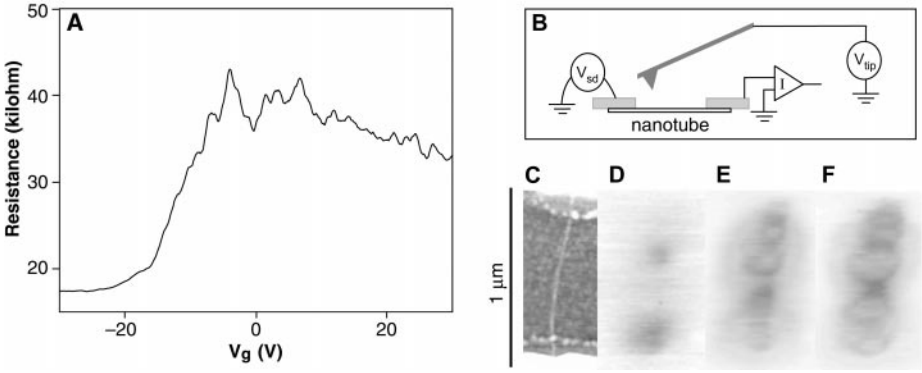

Fig. 1. (**A**) Plot of low-bias resistance of metallic SWNT device D1 as a function of V_g. (**B**) Experimental setup for scanned gate microscopy. *I*, current. (**C**) Topographic image of D1. (**D**) Scanned gate image with $V_{tip} = 3$ V. The dark color indicates increased resistance. (**E**) Scanned gate image with $V_{tip} = 6$ V. (**F**) Scanned gate image with $V_{tip} = 8$ V.

[1]Department of Physics, [2]Department of Chemistry and Chemical Biology, Harvard University, Cambridge, MA 02138, USA.

*To whom correspondence should be addressed. E-mail: HPark@chemistry.harvard.edu

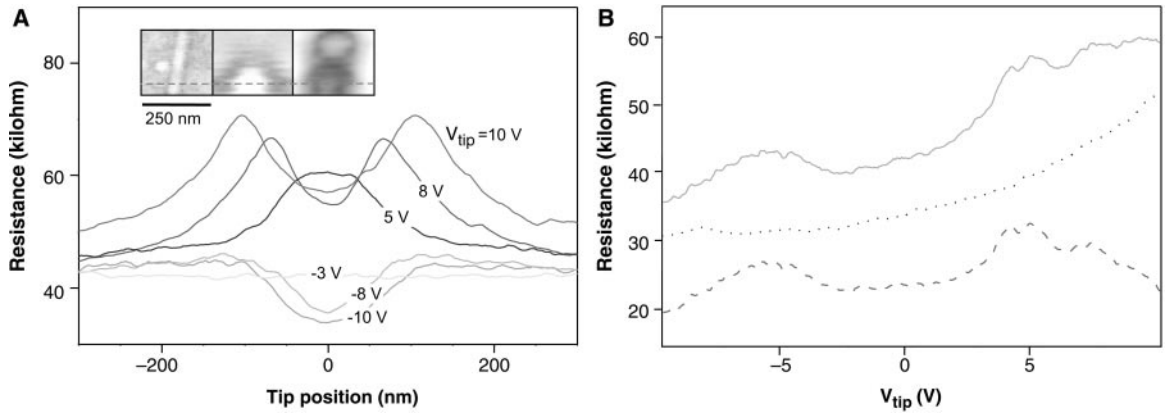

Fig. 2. (**A**) Plots of resistance versus tip position as the tip is scanned through the lower ring (along the dashed line in the inset) at the indicated V_{tip} values. (Inset) The left panel shows the topographic image of a 250-nm SWNT segment in nanotube device D2. The middle panel shows a scanned gate image with $V_{tip} = -9$ V. The right panel shows a scanned gate image with $V_{tip} = 5$ V. (**B**) The solid curve shows the plot of resistance versus V_{tip} at the lower defect; the dotted curve is the scaled plot of resistance versus V_{tip} at the upper defect. The data are scaled along the V_{tip} axis by a factor of 2. The dashed curve is the plot of resistance change due to the lower defect alone. The lower two curves are offset for clarity.

the SG ring indicates that the nanotube resistance reaches a peak when the tip is a fixed distance away from the scattering centers. Examination of AFM images shows that no discernible correlations exist between the AFM topography and the SG ring positions.

The evolution of the SG rings can be examined more quantitatively in Fig. 2. The data were obtained from a device (D2) with a 250-nm nanotube segment connected to electrical leads. The topographic image of the nanotube segment along with two SGM images are shown in the inset of Fig. 2A. As shown in the right SGM image, the device contains two scattering centers separated by ~120 nm.

The resistance-tip position plot that is traced as the tip is scanned through the center of the lower SG ring is shown in Fig. 2A. At low positive V_{tip} values, a single resistance peak (the dark spot in SGM images) appears on the nanotube. As V_{tip} is increased, this resistance peak evolves into two peaks whose separation increases with V_{tip}, mapping the behavior of the SG ring. At large negative V_{tip} values, the resistance of the nanotube drops when the tip is over the nanotube, consistent with the bright spot in the middle panel of the inset in Fig. 2A. This resistance dip was observed only at the lower SG ring and was not observed at the upper SG ring. The resistance-V_{tip} trace obtained with the tip held over the lower SG ring center shows two resistance peaks superposed on a rising background (Fig. 2B).

The tip-position scan in Fig. 2A and the V_{tip} scan in Fig. 2B can be understood by considering how ε_{loc} in the nanotube shifts as V_{tip} and the tip position are varied. In SGM, the local charge accumulation and ε_{loc} are determined by the local electrostatic potential Φ_{loc} along the nanotube (*25, 26*). Although Φ_{loc} is directly proportional to V_{tip}, it falls off with increasing tip-nanotube distance because of the reduced electrostatic coupling. Therefore, decreasing V_{tip} or increasing the tip-nanotube distance has the same effect on Φ_{loc} and ε_{loc} at the center of an SG ring. Consequently, Fig. 2, A and B, shows two different manifestations of the same physical phenomenon: the device resistance exhibits peaks as ε_{loc} is varied near a particular electron scattering center, signifying the occurrence of resonant electron scattering.

This observation constitutes our central experimental finding. One explanation of the observed behavior is external disorder provided by localized charge traps within the substrate or surface contaminants. Theoretical studies have shown, however, that the disorder potential must vary rapidly on a length scale of ~1 Å to affect electronic transport in metallic nanotubes (*27*). Localized charges extrinsic to the nanotube are unlikely to produce such short-ranged disorder. Furthermore, the V_{tip}-induced sequential charging of the extrinsic charge traps would show a single value of the resistance for each charge state, leading to steplike resistance changes in contrast to the resistance peaks in Figs. 1 and 2. These considerations, together with the ubiquity of the observed phenomena in CVD-grown nanotubes, strongly suggest that the resonant electron scattering is due to localized defects intrinsic to the nanotubes.

Previous theoretical studies have shown that structural defects in metallic SWNTs generally lead to resonant electron scattering at energies corresponding to defect states or one-dimensional subband edges (*11, 15–17*). Our experimental observation is fully consistent with these theoretical predictions and suggests the presence of structural defects in CVD-grown nanotubes. Although the SGM images alone cannot provide information on the atomic structure of nanotube defects, the distinct V_{tip} responses of upper and lower scattering centers in device D2 illustrate that more than one type of defect is present in metallic nanotubes.

The data in Fig. 2 provide quantitative information on the electron scattering probability by these defects. Using Landauer-Büttiker formalism and ignoring phase-coherent scattering between defects at room temperature, one can express the total resistance of device D2 as (*26*)

$$R_{total} = R_c + \frac{h}{4e^2}\left(1 + \frac{r_l}{1 - r_l} + \frac{r_u}{1 - r_u}\right)$$

Here, R_c stands for the resistance due to transport barriers at the nanotube-electrode interface, and r_l and r_u designate the electron reflection coefficients of the lower and upper defects, respectively. Within this framework, the resistances of the two defects simply add in series like classical resistors, and V_{tip}-induced resistance changes result from changes in r_l and r_u. Because electrostatic coupling is long-ranged, V_{tip} affects both r_l and r_u, irrespective of the tip position. Information on the distance dependence of tip-nanotube coupling is therefore required to determine the resistance change due to an isolated defect.

This information can be obtained from Fig. 2A. Specifically, it shows that, as the tip-defect distance increases from 0 to 120 nm (the separation between the lower and upper defects), the value of V_{tip} that causes the maximum device resistance changes from 5 to 10 V. This observation suggests that, when V_{tip} is varied with the tip over the lower defect, the shift in ε_{loc} at the upper defect is smaller by a factor $\alpha \sim 2$, compared to that at the lower defect. Therefore, the contribution of the upper defect to the resistance-V_{tip} trace at the lower defect (the solid curve in Fig. 2B) can be approximated by measuring the resistance-V_{tip} trace at the upper defect and plotting it against αV_{tip} (the dotted curve in Fig. 2B). The resistance change due to the lower defect alone can then be obtained by subtracting the dotted curve from the solid curve.

The result of this subtraction (the dashed curve in Fig. 2B) shows two distinct resistance peaks ~10 kilohms in height. These resistance peaks correspond to the electron

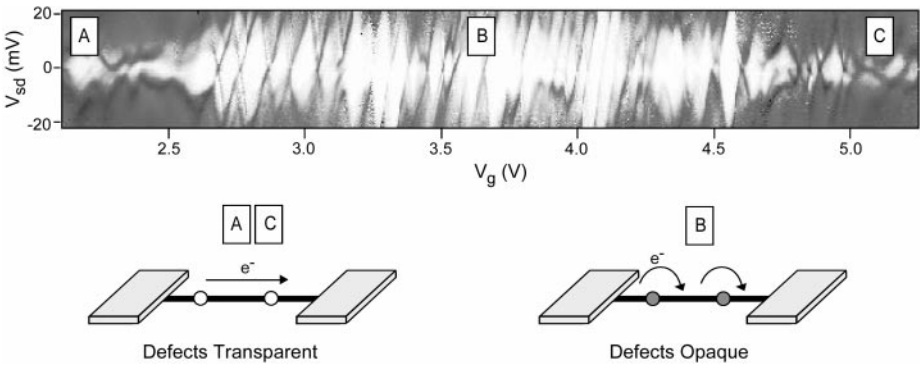

Fig. 3. Gray-scale plot of differential conductance (dI/dV_{sd}) of device D2 as a function of V_{sd} and V_g at $T = 4.2$ K. In this panel, white corresponds to zero conductance, and black corresponds to 40 μS. In regions A and C, the defects in the nanotube are tuned to transparency. In region B, the defects are tuned to result in strong electron scattering.

scattering resonances of the lower defect. If $r_1 = 0$ away from the scattering resonances, the observed resistance change yields $r_1 \sim 0.7$ at the peak of the scattering resonance. Because r_1 may not be zero off resonance, this estimate represents an upper bound for r_1. A similar analysis of defects in other samples indicates that the reflection coefficients of defects range from 0.5 to 0.7 at room temperature. The V_{tip}-induced ε_{loc} change is estimated to be ~50 meV/V from the comparison of the V_{tip} and V_g scans (*28*), which indicates that the resonance peaks in Fig. 2B are separated by ~0.5 eV in their energy positions. Both the value of r and the energy separation between resonances compare favorably with theoretical predictions for various few-atom defects in SWNTs (*11, 15–17*).

The present finding indicates that the defects in metallic nanotubes act as gate-tunable electron scatterers and SWNTs with defects can be the basis for new types of electronic devices (*14*). One example for such devices is demonstrated here by the formation of an intratube quantum dot by two defects. A gray-scale differential conductance plot measured from device D2 at temperature $T = 4$ K is shown in Fig. 3 as a function of V_{sd} and V_g. At the V_g ranges designated as regions A and C, the electron scattering by defects is minimal. In this region, the low-bias conductance of D2 never reaches zero, irrespective of V_g, and the nanotube acts as a metallic wire. In the V_g range designated as region B, on the other hand, defects act as strong electron scatterers, and the nanotube section between two defects turns into a quantum dot, as illustrated by the well-known Coulomb-blockade patterns in Fig. 3 (*29*). This dot exhibits a charging energy around 20 meV, just as expected for a quantum dot that is ~120 nm in length (*3*). Unlike nanotube dots reported previously, the barriers that form the intratube quantum dot can be tuned by adjusting V_g, illustrating the unique potential of defect manipulation in molecular electronic applications of SWNTs.

References and Notes

1. C. Dekker, *Phys. Today* **52** (no. 5), 22 (1999).
2. T. W. Odom, J.-L. Huang, P. Kim, C. M. Lieber, *J. Phys. Chem. B* **104**, 2794 (2000).
3. M. Bockrath *et al.*, *Science* **275**, 1922 (1997).
4. S. J. Tans *et al.*, *Nature* **386**, 474 (1997).
5. S. J. Tans, R. M. Verschueren, C. Dekker, *Nature* **393**, 49 (1998).
6. R. Martel *et al.*, *Appl. Phys. Lett.* **73**, 2447 (1998).
7. J. Kong *et al.*, *Science* **287**, 622 (2000).
8. T. W. Tombler *et al.*, *Nature* **405**, 769 (2000).
9. T. Rueckes *et al.*, *Science* **289**, 94 (2000).
10. J.-C. Charlier, T. W. Ebbesen, P. Lambin, *Phys. Rev. B* **53**, 11108 (1996).
11. L. Chico, L. X. Benedict, S. G. Louie, M. L. Cohen, *Phys. Rev. B* **54**, 2600 (1996).
12. L. Chico *et al.*, *Phys. Rev. Lett.* **76**, 971 (1996).
13. V. H. Crespi, M. L. Cohen, A. Rubio, *Phys. Rev. Lett.* **79**, 2093 (1997).
14. L. Chico, M. P. L. Sancho, M. C. Muñoz, *Phys. Rev. Lett.* **81**, 1278 (1998).
15. T. Kostyrko, M. Bartkowiak, G. D. Mahan, *Phys. Rev. B* **59**, 3241 (1999).
16. ———, *Phys. Rev. B* **60**, 10735 (1999).
17. H. J. Choi, J. Ihm, S. G. Louie, M. L. Cohen, *Phys. Rev. Lett.* **84**, 2917 (2000).
18. P. G. Collins, A. Zettl, H. Bando, A. Thess, R. E. Smalley, *Science* **278**, 100 (1997).
19. Z. Yao, H. W. C. Postma, L. Balents, C. Dekker, *Nature* **402**, 273 (1999).
20. W. Clauss *et al.*, *Europhys. Lett.* **47**, 601 (1999).
21. J. H. Hafner *et al.*, *Chem. Phys. Lett.* **296**, 195 (1998).
22. J. H. Hafner, C. L. Cheung, C. M. Lieber, *J. Am. Chem. Soc.* **121**, 9750 (1999).
23. Degenerately doped silicon wafers with a 1-μm oxide layer were dipped in a 0.1 mM solution of $Fe(NO_3)_3 \cdot 9(H_2O)$ in isopropanol, rinsed in hexane, and then dried. The wafers were placed in a furnace and heated under argon [600 standard cubic centimeters per minute (sccm)] and hydrogen (400 sccm) to the reaction temperature (700° to 900°C). Nanotubes were grown by flowing ethylene at 0.5 sccm for 6 min.
24. M. Bockrath *et al.*, *Nature* **397**, 598 (1999).
25. S. J. Tans, C. Dekker, *Nature* **404**, 834 (2000).
26. A. Bachtold *et al.*, *Phys. Rev. Lett.* **84**, 6082 (2000).
27. P. L. McEuen *et al.*, *Phys. Rev. Lett.* **83**, 5098 (1999), and references therein.
28. The V_g scan (Fig. 3) shows that ~12 electrons per volt are added to the nanotube in the Coulomb-blockade region. The chemical potential change (~50 meV/V) is obtained by multiplying the number of electrons added by the mean level spacing (~4 meV for a 120-nm-length tube, assuming spin degeneracy). The comparison between the V_g and V_{tip} scans shows that a back gate and the AFM tip have similar local electrostatic coupling.
29. H. Grabert, M. H. Devoret, *Single Charge Tunneling* (Plenum, New York, 1992).

30. This work was supported by the Air Force Office of Scientific Research and NIH (C.M.L.), NSF and the Office of Naval Research (M.T.), and the Dreyfus Foundation and Harvard University (H.P.).

5 September 2000; accepted 24 November 2000

A Three-Dimensional Synthetic Metallic Crystal Composed of Single-Component Molecules

Hisashi Tanaka,[1] Yoshinori Okano,[1] Hayao Kobayashi,[1] Wakako Suzuki,[2] Akiko Kobayashi[2]*

Molecular metals normally require charge transfer between two different chemical species. We prepared crystals of $[Ni(tmdt)_2]$ (tmdt, trimethylenetetrathiafulvalenedithiolate) and carried out crystal structure analyses and resistivity measurements. The analyses and measurements revealed that these single-component molecular crystals are metallic from room temperature down to 0.6 kelvin. Ab initio molecular orbital calculations suggested that π molecular orbitals form conduction bands. The compact molecular arrangement, intermolecular overlap integrals of the highest occupied and lowest unoccupied molecular orbitals, and tight-binding electronic band structure calculation revealed that $[Ni(tmdt)_2]$ is a three-dimensional synthetic metal composed of planar molecules.

Semiconducting properties in phthalocyanine and condensed aromatic hydrocarbons were found around 1950 (*1*, *2*), and one-dimensional molecular metals were discovered around 1970 (*3*, *4*). Ever since the discovery of the organic superconductor $(TMTSF)_2PF_6$ (TMTSF, tetramethyltetraselenafulvalene) in 1980 (*5*), an extremely large number of molecular conductors have been developed. Until recently, however, a difficult problem in the metallization of molecular crystals had remained unsolved. In contrast to typical inorganic metals composed of single elements, such as sodium and copper, all of the exam-